Impact-parameter dependence of the energy loss of fast molecular clusters in hydrogen

R. C. Fadanelli and P. L. Grande

Instituto de Física, Universidade Federal do Rio Grande do Sul, Avenida Bento Gonçalves 9500, 91501-970, Porto Alegre, RS, Brazil

G. Schiwietz

Hahn-Meitner-Institut, Abteilung SF8 Glienicker Strasse 100, D-14109 Berlin, Germany
(Received 19 November 2007; published 12 March 2008)

The electronic energy loss of molecular clusters as a function of impact parameter is far less understood than atomic energy losses. For instance, there are no analytical expressions for the energy loss as a function of impact parameter for cluster ions. In this work, we describe two procedures to evaluate the combined energy loss of molecules: *Ab initio* calculations within the semiclassical approximation and the coupled-channels method using atomic orbitals; and simplified models for the electronic cluster energy loss as a function of the impact parameter, namely the molecular perturbative convolution approximation (MPCA, an extension of the corresponding atomic model PCA) and the molecular unitary convolution approximation (MUCA, a molecular extension of the previous unitary convolution approximation UCA). In this work, an improved ansatz for MPCA is proposed, extending its validity for very compact clusters. For the simplified models, the physical inputs are the oscillators strengths of the target atoms and the target-electron density. The results from these models applied to an atomic hydrogen target yield remarkable agreement with their corresponding *ab initio* counterparts for different angles between cluster axis and velocity direction at specific energies of 150 and 300 keV/u.

I. INTRODUCTION

Energy loss and channeling phenomena of molecular and cluster ions are not so well understood as the corresponding phenomena for monoatomic ions. Important cluster-beam applications can be found in the enhanced sputtering process [1–4], in secondary-electron emission enhancement [5], in plasma physics [6], and even in inertial nuclear fusion [7] due to the vastly enhanced cluster energy deposition.

Pioneering work in the decade around 1970 shows that cluster-beam effects deviate clearly from the sum of the separated actions of each part of the cluster. In other words, there is interference among the transitions induced by the different cluster components. This interference was shown for the ion energy loss [8,9]. The energy-loss effects were extensively studied in a review paper [10], which describes the so-called vicinage effect, the nonadditivity of the cluster-component energy losses. Another important cluster phenomenon is the Coulomb explosion [11–19]. While penetrating the target, a swift cluster ion loses a large fraction of its electrons and, then, undergoes a breakup process due to quasi-Coulomb forces among its components. If the clusters enter along a principal crystal axis, their motion will be guided due to the correlated collisions with the target atoms and, the motion of the molecule or its fragments will additionally depend on the Coulomb explosion. Together, channeling and Coulomb explosion phenomena lead to the Coulomb heating mechanism [20–22] that leads to an increase of the kinetic energy of the cluster fragments along the transverse direction of the channel, thus allowing a major change in the channeled cluster-flux distribution, if compared with the channeled monoatomic ion flux.

The electronic energy loss of clusters can be simulated by the united-atom scaling [23], which treats the cluster as an equivalent single atom, with atomic number and mass number being the sum of the individual components' atomic number and mass. However, this oversimplified model could describe successfully only the very beginning of the interaction between the cluster and the target (before the Coulomb explosion is significant) and it is limited to an intermediate velocity range, since neither the asymptotically small nor the large impact parameters are considered correctly. Therefore, several cluster channeling key effects cannot be understood, for instance, the Coulomb heating effect. One of the most accurate models to describe the electronic cluster energy loss is the dielectric formalism for a homogenous electron gas target [8,10,24]. While this type of model describes successfully the electronic cluster energy loss (it can describe explicitly the interference terms), it is not possible to readily use the dielectric formalism for nonuniform electron targets. Hence, as crystalline targets cannot be treated as being homogenous, the channeled cluster energy loss cannot be correctly described by that formalism. Therefore, a theoretical investigation of the cluster stopping power under channeling conditions requires the use of the impact-parameter method as presented by Jensen *et al.* [25]. The impact-parameter method describes the energy transfer Q between the projectile and the target as a function of the impact parameter b, namely $Q(b)$, for a classical projectile trajectory. In the above cited work, however, basically only distant collisions have been considered.

The present work describes and compares two distinct approaches to obtain values for the cluster energy loss $Q(b)$. The first approach consists in two different *ab initio* calculations [26–28], namely the first-order semiclassical approximation (SCA) and the coupled-channel method using atomic orbitals (AO), both of them requiring the use of a large set of electronic quantal target states (typically several hundred). While these *ab initio* calculations achieved high precision

(especially with the AO type), they require a large computational time due to the large set of bound and continuum target-electron states. The second approach is the use of simplified and less detailed models. These simplified models are based on molecular extensions of the perturbative convolution approximation (PCA) [29,30] and the unitary convolution approximation (UCA) [31]. Both PCA and UCA are known as reliable and simple models to obtain $Q(b)$, used in channeling energy-loss simulations. However, PCA and UCA do neglect some interaction phenomena, such as electron capture or the polarization (Barkas) effect [33].

Recently, an extension of the PCA, namely the molecular PCA (MPCA) was developed and the results shows a fairly good agreement with the corresponding molecular first-order SCA calculations [34] for intermediate (about 2 atomic units) inter-projectile-nuclear distances. The time consuming *ab initio* calculations will be used in this work as a benchmark for the molecular versions of the simplified models, especially the unitary model, and comparisons between AO and molecular UCA (MUCA) and between MPCA and molecular PCA will be performed. The results of the electronic cluster energy loss as a function of the impact parameter are given for different cluster geometries. For the simplified models MPCA and MUCA, the large set of electronic states is replaced by oscillator strengths and the target ground-state density (in the present case simply the density for H) as the physical inputs.

II. MODELS

As pointed out in the introduction, the energy transfer as a function of the impact parameter is given by two different types of approaches, namely the *ab initio* calculations (SCA and AO) and the simplified models (MPCA and MUCA). In the following, the atomic-units system ($\hbar = m_e = q_e = 1$) is used.

A. *Ab-initio* calculations

A brief outline of the *ab initio* calculations is given in this section. Consider a system that contains a projectile p (monoatomic ion or a cluster ion) interacting with a target atom t. It is important to point out that for the current approximations the projectile is considered as a classical body. One can, as usual, define the impact parameter b as the minimum distance between the straight-line projectile trajectory (defined by the motion of the monoatomic ion or of the center of the cluster ion) and the target atom. Finally, the target atom contains one or more bound electrons (e). Therefore, the associated Hamiltonian is given by

$$H_e = H_{te}(\vec{r}) + V_{pe}(\vec{R}(t) - \vec{r}), \tag{1}$$

where r is the electron coordinate, R is the distance between the target nucleus and the projectile center, H_{te} is the (unperturbed) Hamiltonian of the system electron-target nucleus [$H_{te}(\vec{r}) = T_e(\vec{r}) + V_t(\vec{r})$, where T_e is the electron kinetic energy operator and V_t is the nucleus-electron potential energy operator of the target] and, finally, V_{pe} is the potential energy operator of the projectile-electron pair. Furthermore,

projectile-centered electronic states will be disregarded.

In what follows, the time-dependent electronic wave function $\Phi_e(\vec{r}, t)$ is expanded using the unperturbed eigenstates of H_{te}, defined in terms of radial functions u and of the spherical harmonics Y_{lm}. Then, the unperturbed states are given by $\phi_{n,l,m}(\vec{r}) = Y_{lm}(\theta, \phi) u_{nl}(r)/r$. Therefore, the following general expression is used:

$$\Phi_e(\vec{r}, t) = \sum_{n,l,m} a_{n,l,m}(t) e^{-i\varepsilon_{n,l}t} \phi_{n,l,m}(\vec{r})$$
$$+ \sum_{l,m} \int_0^\infty d\varepsilon\, b_{l,m}(\varepsilon, t) e^{-i\varepsilon t} \phi_{n,l,m}(\vec{r}). \tag{2}$$

More details of this expansion are given in Ref. [26]. Inserting Eq. (2) into the Schrödinger equation for the electron and subsequent application of the inner product with an arbitrary eigenstate of H_{te} yields the following result:

$$i\frac{d}{dt}a_{n,l,m} = \sum_{n',l',m'} a_{n',l',m'}(t) e^{i(\varepsilon_{n,l} - \varepsilon_{n',l'})t} \langle \phi_{n',l',m'} | V_{pe}(\vec{R}(t) - \vec{r})$$
$$\times |\phi_{n,l,m}\rangle \tag{3}$$

with the boundary condition $a_{n,l,m}(t \to -\infty) = \delta_{1s0,nlm}$. This set of differential equations is known as the coupled-channel equations. The summation over n should be understood as a proper summation for the bound states and as an integration over energy for the continuum states.

The separation between the radial and the angular parts of the eigenstates H_{te} allows the analytical calculation of the angular part of the matrix elements of the potential V_{pe}. Therefore, only the radial part of the matrix elements must be evaluated numerically, as carried out for monoatomic ions in Refs. [26,27].

With the use of all matrix elements, Eq. (3) is used to obtain the coefficients $a_{n,l,m}$ in two different ways. In the first case, in each equation, only the matrix elements involving the ground state and the given final state (n, l, m) are used (the first-order perturbation framework). This procedure removes the coupling among the equations and the resulting form is a set of uncoupled integrals for the coefficients, generally known as the semiclassical approximation:

$$a_{n,l,m} = -i \int_{-\infty}^{\infty} dt \exp[i(\varepsilon_{n,l,m} - \varepsilon_0)t] \langle n,l,m | V_{pe} | n_0, l_0, m_0 \rangle. \tag{4}$$

In the second form, all terms of the summations are used, resulting in a model known as coupled-channel equations using atomic orbitals as defined by Eq. (3). After obtaining the amplitudes, using one form or the other, the energy transfer as a function of the impact parameter is given by

$$Q(b) = \sum_{n,l,m} |a_{n,l,m}(t \to \infty)|^2 (\varepsilon_{n,l} - \varepsilon_{1s}). \tag{5}$$

This expression is valid for both monoatomic ions and molecular ions. The calculations in Refs. [26,27] were restricted to monoatomic ions. Under that condition, the projectile azimuth angle φ was invariant and, therefore, it could be set as

zero. However, in general, the molecular projectile has different azimuth angles for each of its components. To perform SCA and AO calculations for molecules, the use of the azimuthal wave functions components $\exp(im\varphi_i)$ in each matrix element is mandatory. For a diatomic projectile molecule, the potential matrix elements read as

$$V_{ij}(\vec{R}(t) - \vec{r}) \rightarrow V_{1ij}(\vec{R}_1(t) - \vec{r})\exp(i\Delta m_{ij}\varphi_1) + V_{2ij}(\vec{R}_2(t) - \vec{r})\exp(i\Delta m_{ij}\varphi_2), \quad (6)$$

where $\Delta m_{ij} = m_i - m_j$ and φ_i is the ith projectile azimuthal angle, considering the trajectory line as parallel to the z axis and the projectile center as pertaining to the x axis.

B. Simplified convolution models MPCA and MUCA

Now, in what follows, the simplified convolution models will be described. Before discussing the molecular convolution models, a brief outline of the monoatomic PCA and UCA is given.

The perturbative convolution approximation [29,30] and the unitary convolution approximation (UCA) [31] are two models used to evaluate the energy transference between a monoatomic ion and a single target atom. The ion, in these models, moves along a straight-line path. Both models can be summarized by the following expression:

$$Q(b) = \int K(\vec{b} - \vec{r}_\perp) \int_{-\infty}^{\infty} dz \rho(\vec{r}_\perp, z), \quad (7)$$

where K is a kernel function that contains the collision physics and depends on the type of approximation, b is the impact parameter, $r_\perp$ is the projected distance between a given target electron-coordinate point and its nucleus, orthogonal to the incident ion direction of motion, z is the distance along the ion flight direction, and ρ is the target electronic density.

The kernel function, in the PCA model, is a smooth impact-parameter interpolation among the different interaction regimes between the projectile and the target: The dipole approximation (for large impact parameters), the so-called sudden approximation (for intermediate impact parameters), and the close-collision processes (where the target atom potential can be neglected in the process). Further details are given in Ref. [29] and references therein.

The UCA model is obtained by the introduction of the Bloch correction η as an impact-parameter rescaling in the close-collision term. Another way to introduce the same all-over correction factor is by rescaling $t \rightarrow \eta t$ in Eq. (4). In either case, the b integration of $Q(b)$ to obtain S_e results in the well-known Bloch stopping power if $\eta \neq 1$ is used and in the Bethe stopping power if $\eta = 1$. Further details are given in Ref. [31].

Neither PCA nor UCA contains the polarization (Barkas) effect. PCA contains only Z^2 effects (it is a first-order model for target-centered excitation and ionization) and UCA contains higher-order Z^n terms, but only for even n.

The molecular extensions of the convolution models, namely the molecular perturbative convolution approximation and the molecular unitary convolution approximation can be obtained using the same procedure employed in the
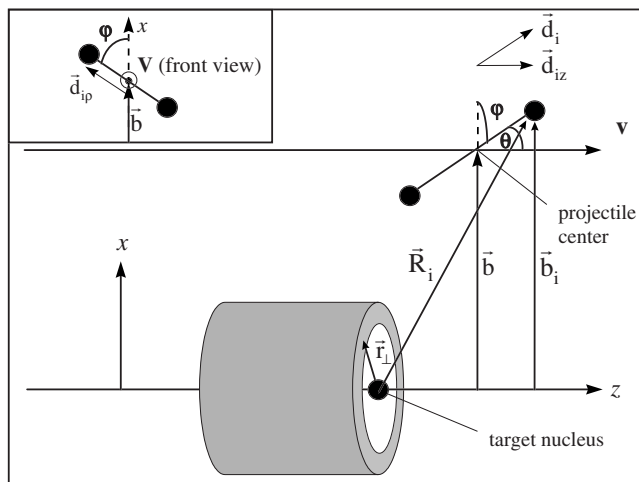

FIG. 1. Schematic plot of the collision geometry. Depicted are the structured projectile with its center, the target nucleus, the target-electron density (integrated along z-axis), the relevant impact parameters, the projectile geometry vectors $\vec{d}$ and, for a diatomic projectile, the characteristic orientation angles θ and φ. The inset shows a front view of the molecule, in order to clarify the meaning of the angle φ.

derivation of their monoatomic counterparts, via the impact-parameter method [25]. Even in the classical calculations, it is clear that the energy transfer has two terms: The sum of the energy transfer by each molecule component and a sum of cross terms, the so-called interference terms.

Let $\vec{r}$ be the distance between the target nucleus and an arbitrary point of its electronic cloud, $\vec{R}_i = \vec{v}t + \vec{b}_i$ is the distance between the target nucleus and the ith cluster ion, $\vec{b}_i = \vec{b} + \vec{d}_i$ is the ith cluster component impact parameter, $\vec{b}$ is the impact parameter of an arbitrary cluster point, and $\vec{d}_i$ is the ith cluster-component position from b. The potential between the electronic cloud and the projectile cluster of velocity v is given by $V = \sum_i V_{\text{ion}}(|\vec{r} - \vec{R}_i|)$. Given a basis of states β, we may recall Eq. (5), for the energy loss, just relabel the energies as ε_0 for the target ground-state energy, and ε_β for the βth state energy.

Figure 1 shows a scheme of the collision system that serves for the description of the relevant terms of a diatomic projectile molecule. The stated problem, then, consists in calculating the probability amplitudes a_β. For a projectile cluster consisting of N ions, we have the following expression assuming linear superposition of amplitudes (as, e.g., within first-order perturbation theory—valid for high projectile velocities):

$$a_\beta^{\text{mol}} = \sum_{k=1}^{N} a_{\beta k} \exp\left(i\frac{d_{zk}}{v}\omega_{\beta 0}\right), \quad (8)$$

where the sum runs for each kth ion of the cluster and, for simplicity, let $\omega_{\beta 0} = \varepsilon_\beta - \varepsilon_0$. By considering the mentioned impact-parameter regions, it is possible to obtain approximate results, valid for each impact-parameter range. The cal-

culations after Eq. (8) are very similar to the ones within the PCA and UCA models. The main difference is the use of the sum of ionic potentials, instead of a single ion potential. Then, it follows that the square modulus of the probability amplitudes will contain cross terms involving phase differences among them, for both close-collision and dipole approximation impact-parameter ranges. Both models result in

$$Q_{\text{MUCA}}(\vec{b}) = \int d^2 r_\perp K_{\text{MUCA}}(\vec{r}_\perp - \vec{b}) \int_{-\infty}^{\infty} dz \ \rho(\vec{r}_\perp, z), \quad (9)$$

formally identical to the PCA and UCA main expressions.

The differences between the atomic and molecular convolution models are easily seen in the kernel function, namely

$$K_{\text{MUCA}}(\vec{b}) = \frac{2}{v^2} \sum_\beta f_\beta \left[\sum_{i=1}^{N} Z_i^2 \left(\frac{g_\perp^2(b_i)}{b_i^2} + \frac{g_\parallel^2(b_i)}{b_i^2} \right) h\left(\frac{2vb_i}{\eta_i} \right) \right.$$

$$+ \sum_{i>j}^{N} Z_i Z_j \cos\left(\frac{\omega_{\beta 0} d_{ijz}}{v} \right) \left(\frac{2\vec{b}_i \cdot \vec{b}_j}{(b_i b_j)^2} g_\perp(b_i) g_\perp(b_j) \right.$$

$$+ \frac{2g_\parallel(b_i)g_\parallel(b_j)}{b_i b_j} \right) \left(h_{\text{trans}}(2vb_i/\eta_i, 2vb_j/\eta_j) \right.$$

$$\left. + \frac{b_i b_j}{\vec{b}_i \cdot \vec{b}_j} h_{\text{par}}(2vb_i/\eta_i, 2vb_j/\eta_j) \right) \right], \quad (10)$$

where the monoatomic terms (first line) and the molecular cross terms (remaining lines) sums are separated for clarity. The function $h(x)$ is given in Ref. [29], corresponding to the close-collision kernel term, $g_\perp$ and $g_\parallel$ are defined in the Appendix, $f_\beta = 2|\langle \beta|z|0 \rangle|^2 (\varepsilon_\beta - \varepsilon_0)$ are the dipole oscillator strengths, $d_{ijz} = |d_{iz} - d_{jz}|$, $\eta_i = \eta(Z_i^{\text{eff}}/v)$ is the Bloch unitary correction [31],

$$\eta_i = \exp\left(\frac{(Z_i^{\text{eff}})^2}{v^2} \sum_{l=1}^{\infty} \frac{1}{l[l^2 + (Z_i^{\text{eff}})^2/v^2]} \right), \quad (11)$$

where Z_i^{eff} is given by

$$Z_i^{\text{eff}} = Z_i + \sum_{j \neq i}^{N} Z_j \frac{\rho(d_{ij\perp}, d_{ijz})}{\rho(0,0)} \quad (12)$$

with $d_{ij\perp} = |\vec{d}_{i\perp} - \vec{d}_{j\perp}|$.

Finally, the functions h_{trans} and h_{par} are the close-collision kernel functions, associated with the electric-fields components induced by the projectile. The terms trans and $\perp$ correspond to the transverse field component, while par and $\parallel$ stand for the field component parallel to the projectile velocity. The close-collision functions are given by

$$h_{\text{trans}}(x_1, x_2) = \frac{x_i x_j}{2} \int_0^1 dq q^2 \sqrt{1-q^2} \cos(2vq^2 d_{ijz}/\eta_{\text{cross}})$$

$$\times [K_1(x_i q^2) J_1(x_j q \sqrt{1-q^2})$$

$$+ K_1(x_j q^2) J_1(x_i q \sqrt{1-q^2})],$$

$$h_{\text{par}}(x_1, x_2) = \frac{x_i x_j}{2} \int_0^1 dq q^3 \cos(2vq^2 d_{ijz}/\eta_{\text{cross}})$$

$$\times [K_0(x_i q^2) J_0(x_j q \sqrt{1-q^2})$$

$$+ K_0(x_j q^2) J_0(x_i q \sqrt{1-q^2})], \quad (13)$$

with K_0, K_1, J_0, and J_1 denoting the Bessel functions in standard notation and $\eta_{\text{cross}} = 2\eta_i \eta_j / (\eta_i + \eta_j)$.

Equation (9), as obtained in this work, accounts for the energy loss of molecular projectiles considering only one target electron. In the independent-particle model framework, MPCA and MUCA can be used if we consider the electronic density and the summed oscillator strengths for each electron on the occupied target shells [see Eq. (10)] and, for Eq. (12), the sum of all electron densities. Thus, the Bloch corrections for the molecular terms should have the same value for all target electrons.

In this way, the Bloch corrections are compatible with the united-atom case, when the distance among the projectile components is much smaller than the characteristic distances inside the target-electron distribution. In that case, regarding the energy loss, the projectile can be treated as a single ion just by summing up its components charge numbers.

The difference between MPCA and MUCA is given by the Bloch unitary correction. If Bloch factors are $\eta_i = 1$ and $\eta_{\text{cross}} = 1$, then we have the MPCA (perturbative) model. Otherwise, Eq. (9) yields the MUCA (unitary) results.

Joining the close collision and the dipole approximation results for the monoatomic terms is a straightforward procedure, already described in Ref. [29]. For the molecular (interference) terms, however, both ranges yield cross terms separated in two parts, namely a part depending on the z-parallel induced field component ($\parallel$) and a part depending on the transverse component ($\perp$). For small impact parameters b_i, the parallel term approaches zero (in either ranges) and the dipole approximation transverse term $g_\perp$ approaches 1. For large impact parameters, the transverse close-collision term h_{trans} approaches 1 and the parallel close-collision term h_{par} approaches 0. Therefore, joining the interference terms for the close collisions and distant collisions is not a straightforward procedure as seen for PCA and UCA models. After analyzing the asymptotic behaviors for each term, we arrive at the ansatz proposed in this work, that takes into account all contributions in the extreme cases of the very small and very large impact parameters, as well as the cluster-component separations. The proposal results in considerable improvements as compared with the one from Ref. [34].

The cosine terms in all interference expressions [Eqs. (10) and (13)] are related to the phase differences among the probability amplitudes of each cluster ion. These terms are related to the Michelson phenomenon of light interference.

Finally, the η_i factor from the Bloch theory is equivalent to an interpolation between the two important energy-loss regimes: The classical Bohr stopping regime of strong perturbations and the quantal first-order Bethe stopping regime (the regime of weak perturbations). For large projectile charges and low velocities, the energy transfer approaches Bohr stopping conditions. For the opposite case it approaches perturbative Bethe conditions.

Here, we have also used the so-called shell corrections or kinematic corrections [35], to take into account the electron velocities in energy-loss processes in close collisions. The MPCA and MUCA close-collisions kernel then must be electron-velocity averaged for each target shell, accounting for the following replacements:

$$\frac{h(2vb_i)}{v^2} \rightarrow \left\langle \frac{h(2vb_i)}{v^2} \right\rangle_{v_e},$$

$$\frac{h_{\mathrm{trans}}(2vb_i, 2vb_j)}{v^2} \rightarrow \left\langle \frac{h_{\mathrm{trans}}(2vb_i, 2vb_j)}{v^2} \right\rangle_{v_e},$$

$$\frac{h_{\mathrm{par}}(2vb_i, 2vb_j)}{v^2} \rightarrow \left\langle \frac{h_{\mathrm{par}}(2vb_i, 2vb_j)}{v^2} \right\rangle_{v_e}, \qquad (14)$$

where the average is performed in the following way for a given function $a(v)$:

$$\langle a(v) \rangle_{v_e} = \int d^3 v_e \frac{\vec{v} \cdot (\vec{v} - \vec{v}_e)}{v|\vec{v} - \vec{v}_e|} f(v_e) a(\vec{v} - \vec{v}_e) \qquad (15)$$

being $f(v_e)$ is the shell velocity distribution and v_e is the target electron velocity for a given shell. However, this is a momentum correction performed in the coordinate space.

In summary, Eq. (9) is the MPCA model, if $\eta_i = 1$ for each i, and is the MUCA model if the Bloch correction [Eqs. (11) and (12)] is taken into account. The corresponding computations are, in comparison with SCA and AO, much more rapid and straightforward. Therefore, the simplified convolution models can be used in energy-loss simulations, whenever fast evaluations of $Q(b)$ are required and one stays in the corresponding range of validity. These ranges of validity will be investigated in detail in the following.

III. RESULTS

In this section, results for the energy loss as a function of the impact parameter are shown for different initial conditions (velocity, nuclear charge, screening) and for different types of approximations. The energy losses for a dicluster and for two uncorrelated atoms are compared, in order to extract the interference effects. If not stated otherwise, the tests are carried out for bare X_2 projectiles (where X is replaced by H, He, Li or the corresponding antiparticle) at an internuclear separation of 2 atomic units (a.u.), corresponding to about 1.06 Å.

In the following we have adapted the subsequent nomenclature convention: SCA, for first-order semiclassical calculations; AO+, for coupled-channel results calculated for a diatomic projectile molecule with positive nuclear charges (this should not be mixed up with the AO+ coupled-channel method [32] based on a wave-function expansion in terms of two nuclear centers plus united-atom states) and finally, AO−, for coupled-channel calculations for a diatomic antimolecule (all collisional parameters are exactly the same as for the AO+ calculations, except for the sign of the projectile charge). Calculations corresponding to the uncorrelated sum
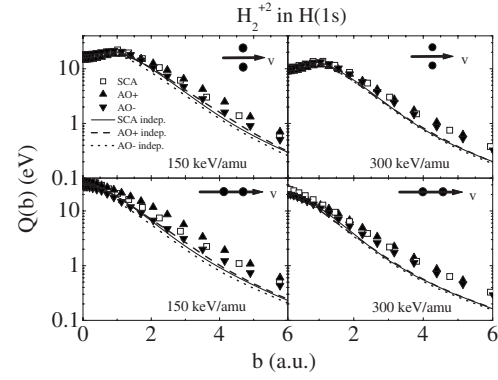

FIG. 2. *Ab-initio* energy-loss results for diatomic H_2^{2+} projectiles for two orientations (depicted near the respective curves) and for two specific energies of 150 keV/amu and 300 keV/amu interacting with an atomic ground-state H target. Open squares stand for the perturbative SCA approximation (independent of the sign of charge). Triangles stand for AO+ (up, for two protons) and AO− (down, for two antiprotons) calculations. The curves correspond to the same type of calculations, however, for uncorrelated projectile particles. For distant collisions, the molecular interference effects can be obtained as the difference between full calculations and independent calculations.

for two projectile atoms are identified by appending the term *independent* to the acronym for the underlying theoretical model.

Figure 2 shows the *ab initio* (SCA and AO) results for H_2^{2+} ions in an atomic H target. For both types of calculations, the projectiles used were the diatomic H_2^{2+} cluster (symbols) and two uncorrelated H atoms with the same individual impact parameters (the curves shown in the plot correspond to an incoherent summation). Two projectile energies (namely 150 keV/amu and 300 keV/amu) and several molecule orientations were employed, but in order to avoid confusion only two of them (parallel and perpendicular orientation) are shown in Fig. 2. The SCA calculations were performed using about 3500 mixed states (both, the so-called gerade and ungerade states with specific angular symmetry) and, due to computational limits, the AO calculations have been restricted to 800 mixed states. Since the interaction potential of the cluster ion has no spherical symmetry, transitions are not restricted to specific wave-function symmetries. First, the SCA results will be briefly analyzed and the AO data will be considered afterwards.

Both top panels show the results for molecules with their axis orthogonal with respect to their motion and parallel to the impact parameter vector. The open square symbols correspond to the molecular SCA results and the continuous curve corresponds to the uncorrelated ions SCA (*independent*). The left-hand panel shows the results for 150 keV/amu and the right-hand panel for 300 keV/amu. For both panels, the pronounced maximum near $b=1$ a.u. is a feature of the reference system used because, for this orientation and $b=1$ a.u., one of the projectile ions undergoes a head-on collision with the target. As discussed before, the interference effects are easily seen as the difference between the SCA and SCA *independent* results and these effects become higher as the impact parameter increases, while the energy dependence

shows a behavior similar to the monoatomic energy one for small impact parameters.

For all orientations, as expected, the perturbative (SCA) energy transfer $Q(b)$ for the uncorrelated pair of projectiles is about 50% smaller than the same results for the molecular projectile at large impact parameters. The perturbative energy transfer depends on the squared projectile charge. For large impact parameters compared to the internuclear separation, the projectile can be viewed as a united ion, with the united-atom charge given by the sum of the individual charges $[Q(b) \propto (Z_1 + Z_2)^2]$. In the opposite case, for close collisions at impact parameters small compared to the molecular components separation, the system approaches a behavior equivalent to the incidence of uncorrelated cluster ions $[Q(b) \propto Z_1^2 + Z_2^2]$. Therefore, a factor of 2 is expected between Q for the molecular and for uncorrelated ions at large impact parameters.

The bottom panels show the results for molecules aligned with their motion. The close-collision behavior is monotonic in this case and the energy losses for small impact parameters are higher than in the previous geometry, as both ions undergo close-collision processes. The interference effects are still clearly seen, mainly for distant collisions.

The same Fig. 2 shows also the AO results. As initially pointed out, AO takes into account all higher-order terms, in particular, the Barkas effect. Therefore, AO calculations for clusters (AO+) and anticlusters (AO−) should be performed in order to better understand the origin of the higher-order effects.

The triangular symbols stand for the AO+ (up) and AO− (down) results. In all panels, the Barkas effect (related to the difference between AO+ and AO− results) is easily seen for distant collisions as expected. The Barkas effect is the dependence of the energy loss on the projectile sign of charge [28,33]. The AO+ energy transfer is larger than the AO− energy transfer for distant collisions. An interesting feature seen in the figure is an increase of the Barkas effect for clusters in comparison with the monoatomic projectiles. By averaging the AO calculations (excluding in this way the Barkas effect), we observe that the more realistic energy-loss result for close collisions is smaller than the SCA results. This is a direct consequence of the electron-number conservation (unitarity) contained in nonperturbative AO calculations and absent in perturbative SCA calculations.

In all panels, AO+ independent and AO− independent results show that the Barkas effect tends toward zero in close collisions for uncorrelated ions. However, for cluster energy losses at small impact parameters, we observe very interesting new features. The top panels, where the molecular geometry permits both ions impinging the target at the same time, but with different impact parameters, show an unexpected "anti-Barkas" effect, i.e., the cluster energy transfer for anticlusters is larger than its cluster counterpart. This could occur due to an antibinding phenomenon. For an anticluster with its axis orthogonal to its motion for close collisions, the antiparticle near the target nucleus weakens the electron-nucleus binding potential for a brief moment. The second antiparticle can, during this process, induce a stronger electronic energy transfer than it would have induced without the other. We call this effect an *assisted* energy transfer. An ana-
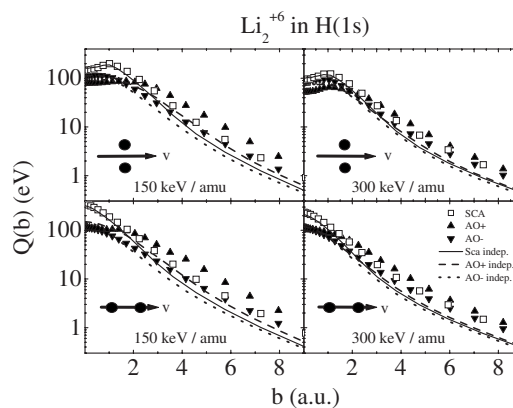

FIG. 3. SCA and AO results for Li_2^{6+} colliding with a ground state H, similar as in Fig. 2. Due to the increased projectile charge, higher-order effects are more pronounced, for instance, antibinding (top left-hand panel) and the difference between SCA and AO calculations for close collisions (bottom left-hand panel).

log argument shows that the positive cluster under the same conditions induces a smaller energy transfer. This is a purely molecular effect and cannot be obtained from monoatomic ions. The bottom panels, showing the molecules aligned with their motion, do not seem to show similar anti-Barkas effects. Contrary, a slight polarization enhancement can be seen in the left-hand bottom panel (150 keV/amu, aligned) for the molecular ion over the uncorrelated protons. It is an indication that the first ion polarizes the target and the second ion, traveling a certain time after the first ion, finds the target already perturbed and polarized. We expect this cluster-induced polarization to maximize for intermediate velocities, corresponding to an optimum repetition period for pulsed excitations (similar as for chirped femtosecond laser pulses).

Both SCA and AO calculations have been also carried out for larger atomic number clusters, namely Li_2. These ions have more intense higher-order effects, due to their higher charge. Figure 3 shows the results for Li_2^{6+}. Both top panels show the results for orthogonal molecule orientation. The anti-Barkas effect at small impact parameters is far easier to visualize in this figure, especially for the 150 keV/amu case. In all cases, it is clear that SCA calculations overestimate all close-collision results due to the aforementioned nonunitarity.

In summary, several nonlinear phenomena, associated to polarization and antibinding, can be seen by comparisons between AO and SCA results. We present the molecular results for both types of calculations. They show the extreme importance of the interference terms. However, both calculations are time consuming due to their heavy computational requirements.

In what follows, the simplified convolution models MPCA and MUCA are compared with the previous SCA and highly reliable AO results, both now used as benchmarks. Figure 4 shows the results for the MPCA energy transfer (accounting for kinematic shell corrections) in a single collision between an H_2 cluster ion and an H target at 300 keV/amu. The top panels display the results for a bare proton dicluster, while the bottom panels stand for a static asymmetric dicluster, namely a correlated H^0-H^+ cluster. It consists of
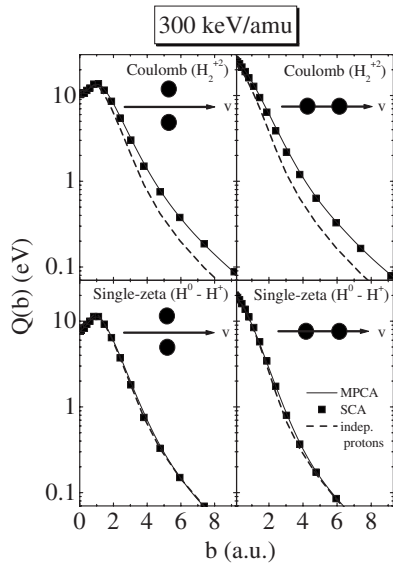
FIG. 4. MPCA results for the energy transfer to an atomic H target induced by 300 keV/amu H_2 diclusters at two different orientations given by the orientation angle θ. The top panels display results for bare fragment protons as projectiles and the bottom panels for fractionally (hydrogenlike) screened protons (see text). The interference contribution can be easily seen in the top panels, while the screening of one ion of the projectile molecule almost eliminates the interference effects, as the intramolecular separation is higher than the screening characteristic length.

a neutral component (described by a single-zeta or hydrogenic screening for unperturbed atomic H) and a Coulombic center (a bare proton). All MPCA results are compared with their SCA counterparts. To emphasize the importance of the interference terms, SCA results for two uncorrelated protons are shown (dashed curves). MPCA results agree fairly well with the molecular SCA results. For the chosen cluster separation (2 a.u.), the improved kernel described in this work shows almost no different results in $Q(b)$, although the original kernel in Ref. [34] should not be used to describe very compact clusters.

A further MPCA test is a direct comparison with the well-established dielectric formalism model [10]. By integrating $Q(b)$ over all impact parameters (as described in Ref. [29]) and by performing an angular average over all molecule orientations, the result is the mean stopping power S. In this way it is possible to obtain the molecular stopping ratio R $= S_{mol}/\Sigma S_{atom}$. The ratio R is obtained from the dielectric formalism as well and can be directly compared with the ratio obtained from MPCA (not MUCA or AO, because the dielectric formalism relies on perturbation theory). These results are seen in Fig. 5 for diatomic H_2 projectiles as a function of the molecular separation for specific projectile energies of 500 keV/amu and 1 MeV/amu. The resonance frequency used in dielectric formalism is the average oscillator strength for the H target and, for comparison purposes, we have performed the MPCA calculations with the same average oscillator strength (without any shell corrections). To within 2%, the averaged MPCA and the dielectric formalism results show a remarkable agreement. We take this as a further confirmation that the perturbative treatment (at least
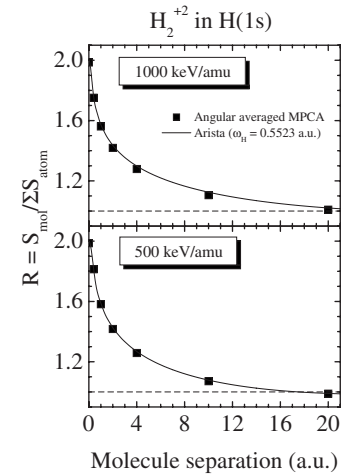

FIG. 5. Stopping power ratios R as a function of the interionic distance for an atomic H target. Note the zero suppression for the vertical R scale. The squares stand for the ratio found using angular averaging and impact parameter integrated results for MPCA. The solid curves stand for the stopping ratio obtained by the use of the dielectric formalism model (Ref. [10]). An overall agreement better than 2% is found between the results of these two perturbative models.

without impact-parameter selection) of ionization and excitation energy losses is well understood.

Figure 6 shows the nonperturbative MUCA results for a bare diatomic hydrogen ion H_2^{2+} in a H target. As in the other figures, two energies and geometries were employed in our tests and MUCA results are compared with AO ones. As MUCA does not contain polarization terms, it should be compared with the average between AO+ and AO− data.

In the top panels of Fig. 6, the results for the orthogonal molecular orientation are shown. In the top right-hand panel (for 300 keV/amu) the accordance between MUCA and AO
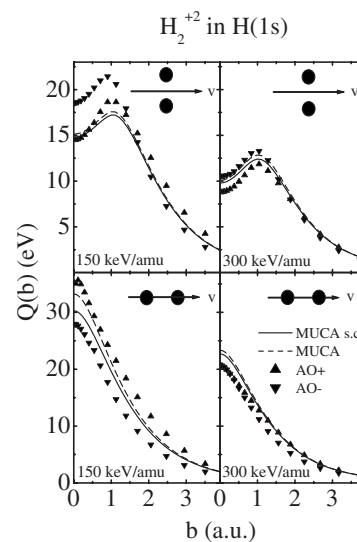

FIG. 6. MUCA results (curves) in comparison with AO results for H_2^{2+} projectile particles (AO+) and antiparticles (AO−). The dashed curves stand for uncorrected MUCA results and the full curves for MUCA with shell corrections (sc).

is fairly good, especially when including shell corrections. The interplay between molecular geometry and projectile-target interaction is correctly taken into account, as can be seen from the maximum of $Q(b)$ around $b=1$ a.u. However, in the left-hand panels (for 150 keV/amu) additional higher-order effects can be seen in the AO results. One of the most important of them, the assisted energy transfer is enhanced for smaller projectile velocities (as already shown in Fig. 2). This can be seen in the AO results as an enhanced splitting between AO+ and AO− at small impact parameters. These nonperturbative effects related to odd orders of the projectile charge (sign-of-charge effects, such as polarization and dynamic binding) are not taken into account in MUCA calculations.

The other important deviation of MUCA data in comparison to charge-averaged AO results for this case is the underestimated energy transfer at small to intermediate impact parameters. The MUCA energy transfer is too low by 10% to 15%, as can clearly be seen in the top left-hand panel. For this case (150 keV/u, $b=0$ to 1 a.u., perpendicular geometry), we have extensively investigated the accuracy of MUCA, MPCA, and PCA (considering the influence of shell corrections) by comparison with SCA and AO benchmark results (not shown here). Comparison of PCA with precision SCA results indicate uncertainties of about ±6% already for the incoherent atomic PCA results (dependent on impact parameter and influenced by the shell correction). The change of the results when replacing the incoherent PCA and SCA calculations by the coherent ones (MPCA and molecular SCA) points to additional uncertainties of about 5% due to the coherence terms. From these numbers we conclude that the difference between MUCA and AO for the top left-hand panel of Fig. 6 is mainly due to the approximations incorporated already in the perturbative PCA and MPCA models. Most likely this is linked to the peaking approximation [29] that is known to become less accurate for smaller velocities and impact parameters. The shell corrections [Eqs. (14) and (15)] do not significantly reduce this uncertainty.

Both bottom panels in Fig. 6 show the results for aligned molecules. MUCA shows a reasonable accordance, slightly improved by the use of kinematic corrections. Even for close collisions at 150 keV/u corrected MUCA results agree very well with the average between AO+ and AO−. In the right-hand panel (for 300 keV/amu), however, even using shell corrections, MUCA still retains a considerable difference to the AO average (at this high velocity, only one-half of this deviation may be due to the peaking approximation discussed above).

One possible explanation for the residual deviation could be given by a "clearing the way" effect [36]. If the molecule is aligned, under close-collision conditions, the first ion would disturb the initial target electronic state by a preionization. Then, the second one would interact with a depopulated state and the net result would be a decreased total energy transfer. However, tests performed with an anti-He-He mixed projectile for AO (not shown here) at two different projectile speeds indicate that it is not the case, since the "clearing the way" effect should be polarity independent (a suppression of the population roughly proportional to Z^2 due to the preionization, resulting in an all-over yield-reduction
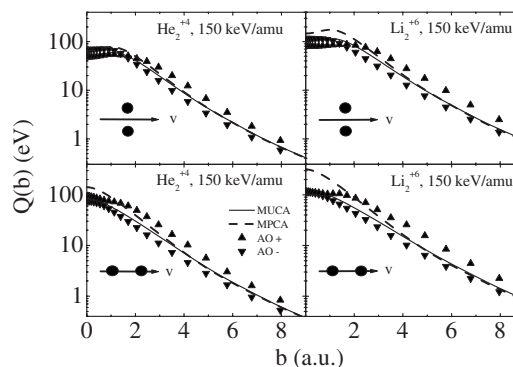

FIG. 7. MUCA results for heavier bare projectiles (He_2 and Li_2). The full curves stand for MUCA results, while the triangles stand for AO+ (up for bare positive ions) and AO− (down for hypothetical antiparticles) calculations. For comparison perturbative MPCA results (dashed curves) are provided. All nonlinear effects previously discussed for H_2 results are now enhanced.

involving a Z^4 contribution). Furthermore, the "clearing the way" effect should be more pronounced at 150 keV/amu, where the ionization cross section is larger.

In fact, the deviations seen in this test are strongly dependent on the projectile polarity and velocity. Therefore, we attribute these deviations to higher-order interference-type effects that have a significant influence on the dynamic evolution of the target electron cloud. One of these effects (consistent with the above-mentioned calculations for dipolar He projectiles) seems to be a focusing of the dynamic electron cloud onto the second projectile constituent (dependent on the electrons inertia and on the sign of charge of the leading particle). This may be viewed as a wake phenomenon, typical also for an electron gas. While AO takes these phenomena into account, MUCA is too simple to include such features. Apart from these effects, however, we expect a better accordance between MUCA and AO results for still higher energies.

Further tests have been performed for heavier bare diclusters, in order to magnify nonlinear effects. Figure 7 shows the results for He_2 and Li_2 at the lower energies (150 keV/amu). All results displayed in this figure include shell corrections. The top panels show He_2 results. Both *assisted energy transfer* (based on binding and antibinding in the top panels) and *cluster-induced polarization* (bottom) are easily seen for AO in close collisions, as discussed before. In general, the accordance between MUCA and AO (after sign-of-charge averaging) is very good. The upper panels display the energy loss for the orthogonal molecule orientation. The disagreement found between averaged AO and MUCA results at small impact parameters in Fig. 6 (for diprotons) is significantly reduced for di-He and changes even its sign for di-Li clusters in this figure. This points to an influence of two different powers of Z in the projectile charge-state dependence for this effect.

The right-hand panels in Fig. 7 show the Li_2 results for bare particle and antiparticle diclusters. For the orthogonal molecule orientation, as well as the aligned molecule, the agreement between MUCA and AO is remarkable. The bottom right-hand panel, however, displays a broad bump struc-

ture for positive Li projectiles (AO+) that is barely visible for lighter positive ions and invisible for negative ones (yet another nonlinear dynamic effect). The same graph shows clearly that MPCA (perturbation theory) can overestimate $Q(b)$ by a factor of 3 for impact parameters smaller than 1 a.u. Therefore, it is clear that MUCA is a real improvement over MPCA, and should be used to estimate the molecular stopping power (especially at lower cluster speeds or for heavier projectile atoms). Contrary, MPCA should be used for comparisons with theoretical perturbative models for clusters, such as the dielectric formalism model [10].

IV. CONCLUSIONS

Energy losses as a function of impact parameter were obtained for projectile clusters from perturbative and from unitary quantal calculations (by the use of hundreds of target states) in this work. Interference effects were explicitly shown, proving that the interaction between molecules and matter cannot be treated by a simple sum of probabilities or cross sections for the individual ions.

Improved simplified models (MPCA and MUCA) were obtained, allowing for a fast and reasonably accurate evaluation of impact-parameter dependent energy transfers, considering several cluster geometries. Reasonable agreement with results from time-consuming benchmark calculations (atomic-orbital coupled-channel method) has been obtained for the impact parameter dependence of the energy transfer. The remaining deviations are mainly related to sign-of-charge effects or to higher-order interference terms dependent on the atomic structure of the cluster, especially for heavier projectile constituents. The main advantage of the simplified models, however, is their high computational speed.

APPENDIX

In this section, the expressions for $g_\parallel$ and $g_\perp$ are stated for three different projectile screening functions. Further information can be found in Refs. [30,34].

For Coulomb potential (no projectile screening), we have

$$g_\parallel(b_i) = \left(\frac{\omega_{\beta0}b_i}{v}\right)K_0\left(\frac{\omega_{\beta0}b_i}{v}\right),$$

$$g_\perp(b_i) = \left(\frac{\omega_{\beta0}b_i}{v}\right)K_1\left(\frac{\omega_{\beta0}b_i}{v}\right). \tag{A1}$$

For Bohr screening, we have

$$g_\parallel(b_i) = \left(\frac{\omega_{\beta0}b_i}{v}\right)K_0\left(b_i\sqrt{\left(\frac{\omega_{\beta0}}{v}\right)^2 + \alpha_i^2}\right),$$

$$g_\perp(b_i) = \sqrt{\left(\frac{\omega_{\beta0}}{v}\right)^2 b_i^2 + \alpha_i^2 b_i^2}\, K_1\left(b_i\sqrt{\left(\frac{\omega_{\beta0}}{v}\right)^2 + \alpha_i^2}\right), \tag{A2}$$

where α_i is the Bohr screening coefficient for the ith screened projectile.

Finally, for single-zeta (hydrogenic) screening, we have

$$g_\parallel(b_i) = \frac{(Z_i - n_i)}{Z_i}\frac{\omega_{\beta0}b_i}{v}K_0\left(\frac{\omega_{\beta0}b_i}{v}\right) + \frac{n_i}{Z_i}\frac{\omega_{\beta0}b_i}{v}K_0\left[\sqrt{\left(\frac{\omega_{\beta0}b_i}{v}\right)^2 + (\alpha_i b_i)^2}\right]$$
$$+ \frac{n_i(\alpha_i b_i)^2}{2Z_i}\frac{\omega_{\beta0}b_i}{v}K_1\left[\sqrt{\left(\frac{\omega_{\beta0}b_i}{v}\right)^2 + (\alpha_i b_i)^2}\right]\bigg/\sqrt{\left(\frac{\omega_{\beta0}b_i}{v}\right)^2 + (\alpha_i b_i)^2},$$

$$g_\perp(b_i) = \frac{(Z_i - n_i)}{Z_i}\frac{\omega_f b_i}{v}K_1\left(\frac{\omega_{\beta0}b_i}{v}\right) + \frac{n_i(\alpha_i b_i)^2}{2Z_i}K_0\left[\sqrt{\left(\frac{\omega_{\beta0}b_i}{v}\right)^2 + (\alpha_i b_i)^2}\right] + \frac{n_i}{Z_i}\sqrt{\left(\frac{\omega_{\beta0}b_i}{v}\right)^2 + (\alpha_i b_i)^2}\, K_1\left[\sqrt{\left(\frac{\omega_{\beta0}b_i}{v}\right)^2 + (\alpha_i b_i)^2}\right], \tag{A3}$$

where n_i is the number of electrons on the ith projectile.

[1] M. Benguerba, A. Brunelle, S. Della-Negra, J. Depauw, H. Joret, Y. Le Beyec, M. G. Blain, E. A. Schweikert, G. Ben Assayag, and P. Sudraud, Nucl. Instrum. Methods Phys. Res. B **62**, 8 (1991).

[2] M. Döbeli, P. W. Nebiker, R. Mühle, and M. Suter, Nucl. Instrum. Methods Phys. Res. B **132**, 571 (1997).

[3] I. Yamada, J. Matsuo, and N. Toyoda, Nucl. Instrum. Methods Phys. Res. B **206**, 820 (2003).

[4] H. H. Andersen, A. Brunelle, S. Della-Negra, J. Depauw, D. Jacquet, Y. Le Beyec, J. Chaumont, and H. Bernas, Phys. Rev.

Lett. **80**, 5433 (1998).

[5] H. Rothard *et al.*, Phys. Rev. B **41**, 3959 (1990).

[6] D. W. Rule and O. H. Crawford, Phys. Rev. Lett. **52**, 934 (1984).

[7] R. J. Beuhler, G. Friedlander, and L. Friedman, Phys. Rev. Lett. **63**, 1292 (1989).

[8] W. Brandt, A. Ratkowski, and R. H. Ritchie, Phys. Rev. Lett. **33**, 1325 (1974).

[9] K. Baudin *et al.*, Nucl. Instrum. Methods Phys. Res. B **94**, 341 (1994).

[10] N. R. Arista, Nucl. Instrum. Methods Phys. Res. B **164–165**, 108 (2000).

[11] D. S. Gemmell, J. Remillieux, J.-C. Poizat, M. J. Gaillard, R. E. Holland, and Z. Vager, Phys. Rev. Lett. **34**, 1420 (1975).

[12] P. Sigmund, Nucl. Instrum. Methods Phys. Res. B **67**, 11 (1992).

[13] M. Farizon, N. V. de Castro Faria, B. Farizon-Mazuy, and M. J. Gaillard, Phys. Rev. A **45**, 179 (1992).

[14] N. V. de Castro Faria, W. Wolff, L. F. S. Coelho, and H. E. Wolf, Phys. Rev. A **45**, 2957 (1992).

[15] M. Farizon, N. V. de Castro Faria, B. Farizon Mazuy, and M. J. Gaillard, Phys. Rev. A **55**, 335 (1997).

[16] M. D. Barriga-Carrasco and R. Garcia-Molina, Phys. Rev. A **68**, 062902 (2003).

[17] S. Heredia-Avalos, R. Garcia-Molina, and I. Abril, Nucl. Instrum. Methods Phys. Res. B **190**, 131 (2002).

[18] Y.-N. Wang, H.-T. Qiu, and Z. L. Mišković, Phys. Rev. Lett. **85**, 1448 (2000).

[19] S. Heredia-Avalos, C. D. Denton, R. Garcia-Molina, and I. Abril, Phys. Rev. Lett. **88**, 079601 (2002).

[20] J. M. Caywood, T. A. Tombrello, and T. A. Weaver, Phys. Lett. **37**, 350 (1971).

[21] T. A. Tombrello and J. M. Caywood, Phys. Rev. B **8**, 3065 (1973).

[22] V. A. Khodyrev, V. S. Kulikauskas, and C. Yang, Nucl. Instrum. Methods Phys. Res. B **195**, 259 (2002).

[23] D. Ben-Hamu, A. Baer, H. Feldman, J. Levin, O. Heber, Z. Amitay, Z. Vager, and D. Zajfman, Phys. Rev. A **56**, 4786 (1997).

[24] N. R. Arista, Phys. Rev. B **18**, 1 (1978).

[25] J. Jensen, H. H. Mikkelsen, and P. Sigmund, Nucl. Instrum. Methods Phys. Res. B **88**, 191 (1994).

[26] G. Schiwietz, Phys. Rev. A **42**, 296 (1990).

[27] P. L. Grande and G. Schiwietz, Nucl. Instrum. Methods Phys. Res. B **132**, 264 (1997).

[28] P. L. Grande and G. Schiwietz, ″Ionization and energy loss beyond perturbation theory,″ *Advances in Quantum Chemistry* (Elsevier, Amsterdam, 2004), Vol. 45, p. 8.

[29] P. L. Grande and G. Schiwietz, Phys. Rev. A **58**, 3796 (1998).

[30] G. de M. Azevedo, P. L. Grande, and G. Schiwietz, Nucl. Instrum. Methods Phys. Res. B **164–165**, 203 (2000).

[31] G. Schiwietz and P. L. Grande, Nucl. Instrum. Methods Phys. Res. B **153**, 1 (1999).

[32] W. Fritsch and C. D. Lin, Phys. Rep. **202**, 1 (1991).

[33] W. H. Barkas, W. Birnbaum, and F. M. Smith, Phys. Rev. **101**, 778 (1956).

[34] R. C. Fadanelli, P. L. Grande, and G. Schiwietz, Nucl. Instrum. Methods Phys. Res. B **230**, 17 (2005).

[35] P. Sigmund, Phys. Rev. A **26**, 2497 (1982).

[36] J. Jensen and P. Sigmund, Phys. Rev. A **61**, 032903 (2000).